Research Article • DOI: 10.2478/s13380-012-0019-8 • Translational Neuroscience • 3(2) • 2012 • 123-131

Translational Neuroscience

VERSITA

Springer

ENTORHINAL VERRUCAE CORRELATE WITH SURFACE GEOMETRY

Jean C. Augustinack[1,*],
Kristen E. Huber[1],
Gheorghe M. Postelnicu[2],
Matthew P. Frosch[3],
Rudolph Pienaar[1,4],
Bruce Fischl[1,5]

[1]*Athinoula A. Martinos Center, Department of Radiology, MGH, 149 13th Street, Charlestown MA 02129 USA*
[2]*Google, Inc. 110 Brandschenkestrasse 8002 Zurich, Switzerland*
[3]*C.S. Kubik Laboratory for Neuropathology, Pathology Service, MGH, 55 Fruit St., Boston MA 02115 USA*
[4]*Fetal-Neonatal Neuroimaging and Development Science Center, Children's Hospital, 300 Longwood Ave, Boston, MA 02115 USA*
[5]*MIT Computer Science and AI Lab, Cambridge MA 02139 USA*

Received 05 April 2012
accepted 11 May 2012

Abstract

Entorhinal verrucae are unique, small elevations on the surface of entorhinal cortex, formed due to distinctive clustering of large neurons in entorhinal layer II. In Alzheimer's disease, the verrucae atrophy as a result of neurofibrillary tangle formation and concomitant neuronal loss. Previously, we found significant decreases in verrucae height, width, surface area, and volume even in the mildest stage of Alzheimer's disease. In this report, we introduce a new method for analyzing verrucae prominence using measures of their curvature. Smoothed surfaces and curvatures were generated using FreeSurfer (http://surfer.nmr.mgh.harvard.edu) from 100 μm^3 *ex vivo* MRI isosurfaces. We examined the positive and negative components of mean curvature AreaNorm($H^{+/-}$) and Gaussian curvature AreaNorm($K^{+/-}$) in entorhinal cortex. A significant difference was found between entorhinal (n=10) and non-entorhinal cortices (n=9) for both AreaNorm($H^{+/-}$) and AreaNorm($K^{+/-}$). We also validated our curvature analysis through a comparison with previously published verrucae measures derived from manual labels of individual verrucae. A significant positive correlation was found between mean verrucae height and AreaNorm($H^{+/-}$). Both mean verrucae height and volume were significantly positively correlated with AreaNorm($K^{+/-}$). These results demonstrate that *K* and *H* are accurate metrics for detecting the presence or absence of entorhinal verrucae. Curvature analysis may be a useful and sensitive technique for detecting local surface changes in entorhinal cortex.

Keywords

• Neuroimaging • Parahippocampal • Curvature • Cortex • Ex vivo • Surface reconstruction • Gaussian • Mean • 3D

INTRODUCTION

Entorhinal verrucae are a unique surface structure on the anterior parahippocampal gyrus. The entorhinal verrucae create a protrusion or bump on the entorhinal surface presumably due to the large neurons that lie beneath the surface in layer II. Retzius and later Klinger described these bumpy structures as the 'verrucae hippocampi' [1,2]. Since they are visible to the naked eye, several scientists have noted their presence [2-6], and in more recent work, the surface elevations have been referred to as the 'entorhinal verrucae', which more accurately describes their location. The quantitative height of an individual verruca was demonstrated to be 0.13 mm for cognitive controls, with a range of 0.25 mm to 0.11 mm in height [3]. From our previous work, verrucae height correlated most strongly with qualitative observations, while verrucae volume was also significantly correlated, but verrucae width and surface area did little to differentiate the elevations from the underlying cortex. In non-demented aging, verrucae increase in total number with increasing age, but decrease in surface area in a cross-sectional study [4]. Conversely, in Alzheimer's disease, the entorhinal verrucae disappear completely due to the massive cortical atrophy. Even in the earliest stages of Alzheimer's disease, a significant decrease in verrucae height, volume, surface area, and width has been demonstrated [3]. For these reasons, entorhinal verrucae make an appealing morphological structure to study in normal controls as well as the Alzheimer's disease population.

The aim of this study was to determine if our previously published manual measurements of individual entorhinal verrucae correlate with curvature functions that survey the entire cortical surface. The process of evaluating entorhinal curvature will be more streamlined than manual measurements, but more importantly will provide additional information about the bumps and the troughs in entorhinal cortex. The relationship between the bumps and troughs will be a novel analysis because the troughs were not incorporated in our previous manual measurements that examined verrucae only. Moreover, a curvature analysis will demonstrate different types of curvatures that identify the entorhinal verrucae. Identification of curvature patterns in *ex vivo* analysis and subsequent validation will help elucidate what the verrucae represent in the normal population.

Differential geometry is the mathematics of idealized surfaces and can be applied to biological surfaces [7]. Geometric surface properties can be separated into two forms: intrinsic and extrinsic. Extrinsic properties depend on the configuration of the particular surface as it is embedded in a space, and as it is apparent to an external observer. Intrinsic properties are invariant of the embedding of

* *E-mail: jean@nmr.mgh.harvard.edu*

the surface in a space and are apparent to a viewer inside the surface [7-10]. The cerebral cortex contains both intrinsic and extrinsic curvatures [9]. A cortical fold, for example, has both extrinsic properties (its general cylindrical shape) and intrinsic properties (the shear and stretch of local features on the fold). It has been documented that intrinsic curvature detects spherical structures – either concave or convex, whereas extrinsic curvature follows every point and changes depending on shape [7,9-11].

Although several studies have examined cortical folding and gyrification to better understand evolutionary and developmental changes [11-14], cortical shape [7,11,15-20] and changes in diseases such as Alzheimer's, autism, depression and schizophrenia [15,16,21-28], none have examined curvature of a specific area and structure at such a high resolution. Our goal was to examine the entire surface curvature in entorhinal cortex (not just the verrucae themselves) with intrinsic and extrinsic curvature measures. Our main objective was to determine whether Gaussian curvature (an intrinsic surface property) and mean curvature (an extrinsic surface property) had an association with previously obtained manual verrucae measurements. With this method of curvature analysis, more subtle surface changes can be detected and described, not only the verrucae but the troughs and saddles (midpoints) as well. In this study, we seek to validate the curvature functions of entorhinal cortex generated using FreeSurfer with our quantitative individual verrucae measurements in cognitive controls. Our quantitative measures included height, volume, surface area and width [3] and the FreeSurfer output included area normalized surface integral functions based on the Gaussian (*K*) and Mean (*H*) curvatures.

EXPERIMENTAL PROCEDURES

Brain Samples

Brain specimens were collected from the Massachusetts General Hospital Autopsy Suite. Ten entorhinal cortex samples were obtained as well as nine other cortical areas that included motor (n=4), orbitofrontal (n=1), Wernicke's area (n=1), occipital (n=1), fusiform area (n=1), and cingulate cortex (n=1) for a total of n=19. All of the samples in this study were clinically cognitively normal and had no cerebrovascular incident or neuropsychiatric history, except one case had history of mild dementia. Additional demographic information has been noted in a previous study [3]. Cases were additionally screened for rapid progressive dementia (Creutzfeldt-Jakob disease), hepatitis and human immunosuppressive virus and, if found, were excluded from this study. The ages ranged from 43-86 and the mean age was 62.71 ± 13.85 years. Our sample set included four females and four males with two cases for which gender information was unavailable. The post-mortem interval for all cases was less than 25 hours.

Ex vivo MRI acquisition

Magnetic resonance images were acquired on a 7.0 T whole body scanner (Magnetom, Siemens Medical Systems, Erlangen, Germany). The radio frequency coil used to acquire the images was a 4-turn solenoid with an inner diameter of 28.5 mm and length of 44 mm. A fast-low-angle-shot (FLASH) sequence was utilized to attain high resolution isotropic (100 μm) voxels with the following parameters: field of view=52 mm (512x512 matrix), slab thickness=25.6 mm (256 partitions), TR=20 ms, TE=7.8 ms, bandwidth =134 Hz/pixel, scan duration = 43min 41sec, full Fourier encoding. Flip angles 10°, 20° and 30° degrees were acquired and isosurfaces were created from three averages at flip angle 20°. All samples were placed in hydrogen free Fomblin (Solvay, Houston, TX, USA) during scanning to produce a clean isosurface not obscured by adjacent liquid. Digital photographs were taken using a Canon Digital Rebel XT camera (Figure 2A).

Manual Verrucae Measures

In our previous study, isosurface models were reconstructed from high resolution *ex vivo* MRI volumes scanned at high field (7.0T) and individual verruca were measured quantitatively for height, width, volume, and surface area on control cases (n=10 cases) [3]. Individual verrucae were systematically

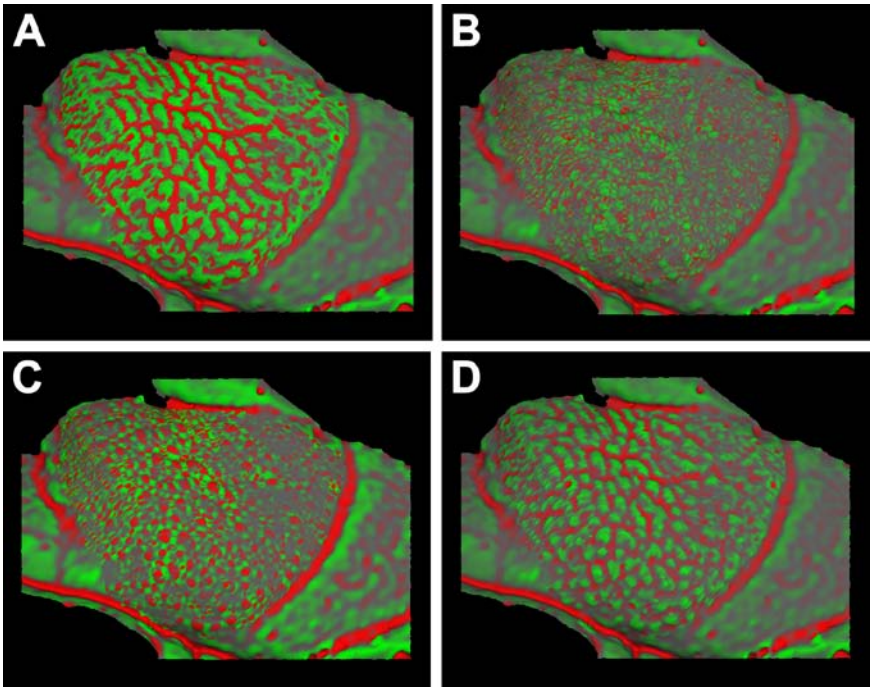

Figure 1. Curvature maps of the entorhinal cortex in the same case. (A) and (B) represent the principal curvatures, k_1 and k_2, respectively. (C) and (D) denote the Gaussian, *K,* and mean, *H,* (unsmoothed) curvature, respectively. Note the red and green colors have different meanings in intrinsic (Gaussian) and extrinsic (mean) surface properties in (C) and (D), respectively. In *H* surfaces, red means depressions or sulci, whereas in *K* surfaces the red color means spherical inference regardless of sign ($^+$ or $^-$, i.e. can be convex or concave). Note the red verrucae highlighted as spherical structures in (C) and green verrucae as maxima in (D).

and randomly labeled on entorhinal surfaces and random patches were labeled on non-entorhinal surfaces. Mean verrucae height for entorhinal surfaces was significantly different from other cortical heights such as, cingulate, frontal, occipital, parietal and temporal cortices. These manual measurements of verrucae were used in this report for validation.

Surface Reconstruction

Isosurfaces were reconstructed from 100 μm^3 *ex vivo* MRI using Freeview which is part of the FreeSurfer package (http://surfer.nmr.mgh.harvard.edu). FreeSurfer uses components of differential geometry to connect multiple vertices that generate the 3D tessellated structure into a smoothed surface (not an isosurface) [29-31]. Here we generated our surfaces using the Marching Cubes algorithm [32] in Freeview.

Curvature Measures

For our analyses, we used tools in FreeSurfer to calculate multiple curvature measures (Figure 1) including the two principal curvatures (k_1 maximum, k_2 minimum) (Figure 1A and 1B), respectively, illustrated in the entorhinal cortex. The Gaussian curvature (K) is the product of the principal curvatures, $K = k_1 k_2$ (Figure 1C) and the mean curvature (H) is the average of the principal curvatures, $H = ½ (k_1+k_2)$ (Figure 1D) [7]. Although based on the same principal curvatures, the two measures, H and K, determine very different geometric properties. The mean curvature is an extrinsic measure and corresponds to what most people visualize when thinking of curvature (i.e. the curved shape of a surface). The mean curvature is measured in units of mm^{-1}. The Gaussian curvature is measured in units of mm^{-2} and is an intrinsic property of a surface that is quite separate from its extrinsic curvature. In the simplest sense, the extrinsic curvature is the curvature apparent to an observer outside of the surface, while the intrinsic curvature is the curvature apparent to an observer inside the surface. The Gaussian curvature can also be thought of as a measurement of differential expansion of a surface. Imagine first a flat surface that "grows" uniformly in all directions; it will remain flat and have zero Gaussian curvature. Imagine now that the center of the surface grows at a faster rate: this will induce a "bubble" in the surface similar to a hemisphere – accumulating positive Gaussian curvature on the bubble. If instead the edges grow faster than the center, a hyperbolic (saddle shaped) surface results, and collects negative Gaussian curvature. In this manner, the Gaussian curvature tags regions of spherical or hyperbolic shape on a surface. It has been speculated that the Gaussian curvature could represent weak points in the surface where stretching occurs [10].

These aforementioned types of curvature were displayed (Figure 1) and each curvature was illustrated in the same case. Note that visually, the K (Gaussian) and the H (mean) curvatures emphasize different aspects of the surface (Figure 1C and 1D), respectively. The H curvature conforms to our intuitive notion of geometry (i.e. Figure 1D), and highlights the tracts of sulci and gyri on the surface that have generally cylindrical shapes. For H, following FreeSurfer convention, green colors denote gyral ridges, and red colors denote sulcal depths. The K curvature image shows quite different surface detail (Figure 1C). For K, the gyral/sulcal folds were less evident; instead we clearly see the entorhinal cortex bumps which conform to a spherical shape and are clearly highlighted as these denote areas of local stretching on the surface.

Area Normalization

For each point on our surface, we multiplied the curvature measure with the area of the mesh that the curvature subtends. This can then be normalized again by the area of the surface to result in a surface area normalized measure, the AreaNorm, which allows for better comparisons between different samples than just comparing raw K and H values. AreaNorm is a FreeSurfer specific term that takes into account the area that was labeled. In this paper, the *positive* integral implies that the AreaNorm calculation was only performed where the respective curvature function was positive; similarly the *negative* integral implies the AreaNorm calculation was only performed where the curvature function was negative. For

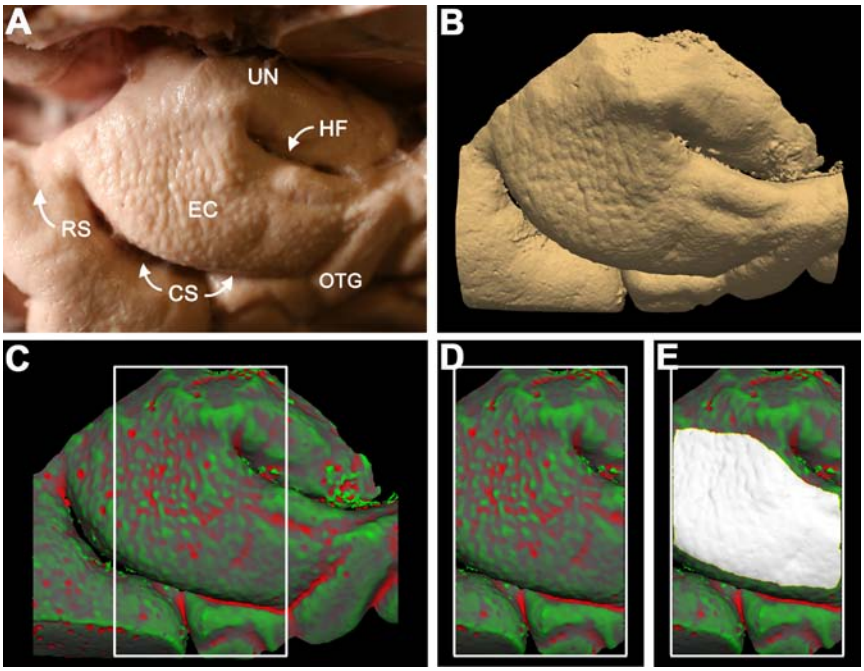

Figure 2. Ventromedial view of the anterior parahippocampal gyrus shows the entorhinal verrucae on the surface in a gross photograph (A). The same view but an isosurface was reconstructed from high resolution *ex vivo* MRI (B). Based on the isosurface in (B), the mean curvature function (*H*, smoothed) was generated in FreeSurfer. White box (C and D) represents our region of interest for the curvature functions presented in the following figures. Our region of interest was confined to entorhinal cortex at all levels of the amygdala. Labels were limited to gyral crowns only (E).

ease of reporting, all integrals were constructed by multiplying area values with the absolute value of the specific curvature function (i.e. all AreaNorm values were reported as positive).

Region of Interest and Manual Labeling

Our methods pipeline is outlined in Figure 2. On intake, we photographed all fixed brain samples with a high resolution Canon camera (Figure 2A). The case illustrated in (Figure 2) has many small entorhinal verrucae on the anterior parahippocampal surface. As described in our previous study [3], we generated isosurfaces from our *ex vivo* MRI for all cortical areas examined. An individual isosurface of entorhinal cortex is shown in (Figure 2B). Subsequently, we generated surfaces on which we projected point-by-point curvature values. In the case of the *H* curvature (Figure 2C and D) the red denotes concave curvature points and is expressed with a positive sign (i.e. sulci and troughs) and the green color implies convex curvature and is expressed with negative curvature (i.e. gyri or verrucae). For *H*, the sign simply indicates the sense of concavity as seen by an external observer. The same shape is positive or negative depending on whether it curves upwards or downwards. In the case of the *K*, however, the red (positive) denotes a different shape (bump, or spherical) than the green (negative, or a saddle shape) irrespective of whether the particular shape is up or down. Given the relative spatial locations of the bumps in the entorhinal cortex, the green (negative) for *H* and the red (positive) for *K* fall on generally the same locations on the entorhinal cortex.

We restricted the region of interest to the anterior most portion of parahippocampal cortex (i.e. anterior 1/3 of entorhinal cortex) so that our measurements were consistent with previous quantitative studies. Specifically, the region of interest included entorhinal slices that contained amygdala as a landmark, even at the most rostral and caudal ends, shown outlined with the white box in Figure 2C, D and E. Panels C and D show the projection of the raw *H* curves on the surface. We drew a label (Figure 2E) using Freeview that included the entire region of interest (white box) but excluded neighboring sulci and any surface artifacts (bubbles or tissue debris) within the region of interest so that only verrucae curvature was analyzed. All cases underwent this procedure to yield the FreeSurfer curvature measures. In this report, we will denote the AreaNorm of the positive mean, *H*, as AreaNorm(H^+), that of the negative mean as AreaNorm(H^-); similarly for the Gaussian, we have AreaNorm(K^+) and AreaNorm(K^-). The combined notation AreaNorm($H^{+/-}$) denotes both AreaNorm functions.

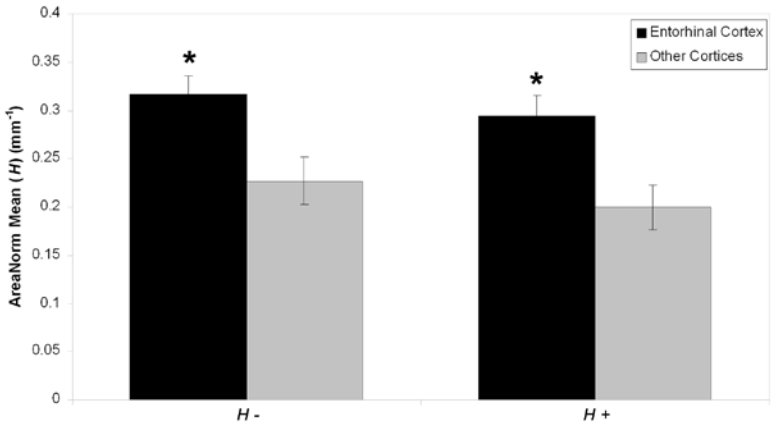

Figure 3. Mean (*H*) curvature in different types of cortex. Bar graph displays AreaNorm($H^{+/-}$) difference between entorhinal cortex (bumpy surface) and other non-entorhinal cortical surfaces (without bumpy surface). Non-entorhinal cortices contain motor cortex (n=4), orbitofrontal cortex (n=1), occipital cortex (n=1), Wernicke's area (n=1), fusiform cortex (n=1) and cingulate cortex (n=1). Note the significant difference between types of cortex for AreaNorm(H^-) (n=19, p= 0.009) and AreaNorm(H^+) (n=19, p= 0.007).

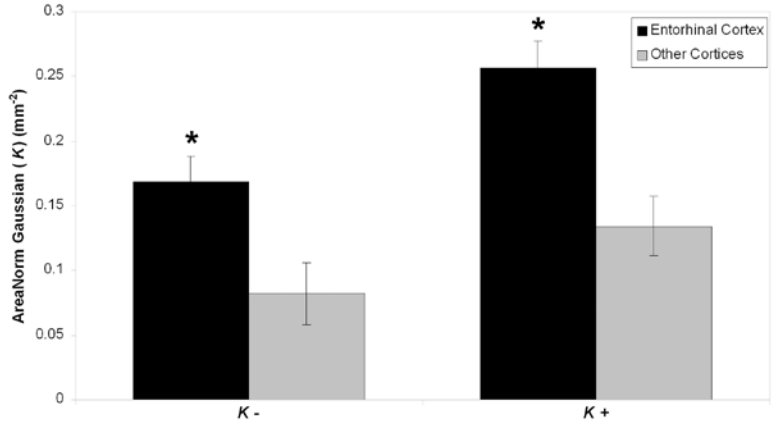

Figure 4. Gaussian (*K*) curvature in different types of cortex. Bar graph shows AreaNorm($K^{+/-}$) difference between entorhinal cortex (bumpy surface) and other non-entorhinal cortical surfaces (without bumpy surface). Non-entorhinal cortices contain same cortices listed in Figure 2. These values were significantly different between types of cortex for AreaNorm(K^-) surface integral (n=19, p=0.009) and the AreaNorm(K^+) surface integral (n=19, p= 0.018).

Statistical Analysis

Pearson's correlation coefficient was used to compare manual verrucae measurements (quantitative height and volume) with the AreaNorm(H^+), AreaNorm(H^-), AreaNorm(K^+) and AreaNorm(K^-). A Mann-Whitney U test was used to compare entorhinal cortex with other cortical areas for AreaNorm(K^+) and AreaNorm(K^-). An independent samples *t*-test was used to compare AreaNorm(H^+), AreaNorm(H^-) between entorhinal cortex and other cortices.

RESULTS

In this study, we compared AreaNorm($H^{+/-}$) and AreaNorm($K^{+/-}$) to our previously published quantitative entorhinal verrucae that were individually and manually labeled [3]. The fundamental workflow for curvature measures is illustrated in Figure 2, and shows the gross specimen, isosurface, smoothed surface, region of interest and label used to generate these subsequent data.

We examined the curvature of non-entorhinal cortex surfaces including motor (Brodmann's area 4), orbitofrontal cortex (Brodmann's area 11), Wernicke's area (Brodmann's area 39), occipital cortex (Brodmann's area 17), fusiform cortex (Brodmann's area ~37 and 20), and cingulate cortex (Brodmann's area 24) with our surface of interest, entorhinal cortex, that contains verrucae (Brodmann's area 28). We included both isocortical areas as well as limbic cortex in our non-entorhinal cortices. The AreaNorm(H^-) was computed to be 0.32 ± 0.02 mm^{-1} in entorhinal cortex and in other cortices (motor, occipital, parietal, frontal, and cingulate), the AreaNorm(H^-) was 0.23 ± 0.02 mm^{-1} (Figure 3). The AreaNorm(H^+) for entorhinal cortex had a mean of 0.29 ± 0.02 mm^{-1} and for the other cortical areas (motor, occipital, parietal, frontal, and cingulate) the AreaNorm(H^+) was 0.20 ± 0.02 mm^{-1} (Figure 3). The AreaNorm(H^-) was significantly different between entorhinal cortex and other cortical areas (p=0.009, n=19, independent samples t-test) and AreaNorm(H^+) was significantly different as well (p=0.007, n=19, independent samples t-test) (Figure 3).

We also evaluated the Gaussian (K) curvature in entorhinal and non-entorhinal regions. The AreaNorm(K^-) was found to have a mean of 0.17 ± 0.02 mm^{-2} in EC, and 0.08 ± 0.02 mm^{-2} in other cortical regions, while the AreaNorm(K^+) had a mean of 0.26 ± 0.03 mm^{-2} in entorhinal cortex, and 0.13 ± 0.04 mm^{-2} elsewhere in cortex (Figure 4). The AreaNorm(K^-) was significantly different between entorhinal cortex and other cortical areas (n=19, p=0.009, Mann-Whitney U), as was AreaNorm(K^+) (n=19, p=0.018, Mann-Whitney U) (Figure 4). In a Gaussian curvature sense, K^+ represents a spherical shape, i.e. the verrucae, while K^- represents a saddle shape. For the entorhinal cortex, the H^- and the K^+ both distinguished the entorhinal (i.e. verrucal) surface from other cortices that do not exhibit verrucae.

We used the same ten cases as in [3] and generated H and K measures for all entorhinal cortices (H, smoothed, Figure 5). To test the entorhinal FreeSurfer curvature as a means for semi-automatically detecting verrucae in *ex vivo*, we used our manually labeled and validated verrucae labels and we compared curvature to verrucae height (mm), verrucae volume (mm^3), verrucae width (mm) and verrucae surface area (mm^2) [3]. The AreaNorm(H^-) was significantly positively correlated with mean verrucae height (n= 10, p=0.009, Pearson's correlation coefficient 0.768) (Figure 6A); the AreaNorm(H^+) was also positively correlated with mean verrucae height (n= 10, p=0.029, Pearson's correlation coefficient 0.684) (Figure 6B) but less so than the AreaNorm(H^-). While both AreaNorm(H^+) and AreaNorm(H^-) were significant for verrucae

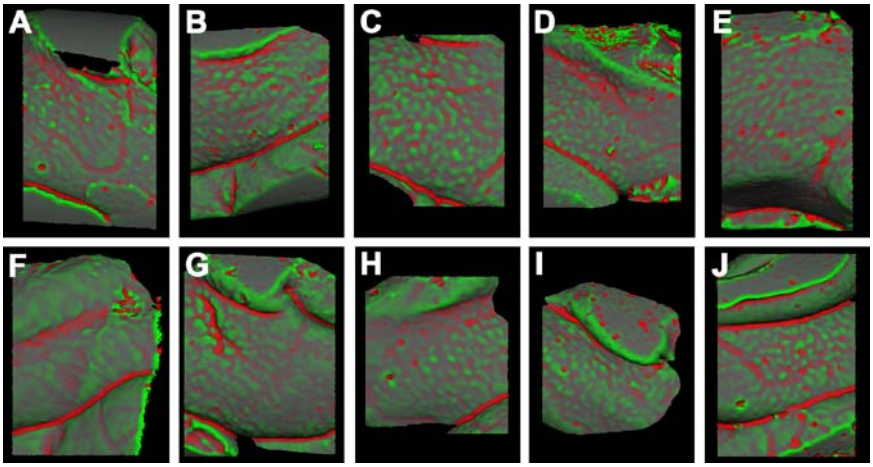

Figure 5. All entorhinal samples displayed as smoothed mean curvatures. Age and gender listed for each case (A) n/a, F, (B) 65yr, M, (C) 67yr, M (D) 50yr, F (E) n/a (F) n/a (G) 60yr, M (H) 86yr, F, (I) 68yr, M (J) 43yr, F. yr = year, M = male, F = female.

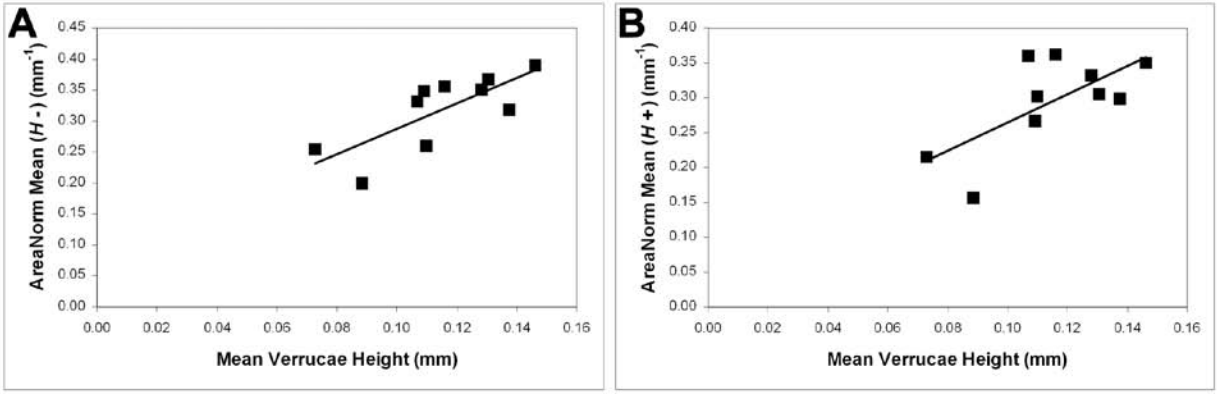

Figure 6. AreaNorm($H^{+/-}$) curvatures correlate to verrucae height. Both positive and negative AreaNorms showed a significant correlation with verrucae height. Correlation for AreaNorm(H^-) and verrucae height was highly significant (p=0.009) (A) while the AreaNorm(H^+) was modestly significant with height (p=0.029) (B). Mean curvature (H^-) represents the verrucae (bumps) loosely while mean (H^+) indicates troughs in between verrucae.

height, the outcome measures of verrucae volume, width and surface area were not significantly correlated (data not illustrated).

The AreaNorm functions of the Gaussian curvature revealed a significant correlation with *both* verrucae height and verrucae volume (Figure 7). The AreaNorm(K^+) and mean verrucae height showed a significant positive correlation (n= 10, p=0.007, Pearson's correlation coefficient = 0.784) (Figure 7A) and the AreaNorm(K^-) also showed a significant positive correlation with height (n= 10, p=0.005, Pearson's correlation coefficient = 0.806) (Figure 7C). The AreaNorm(K^+) was also significantly positively correlated with verrucae volume (n= 10, p=0.045, Pearson's correlation coefficient = 0.644) (Figure 7B) and the AreaNorm(K^-) also showed a significant positive correlation with mean verrucae volume (n= 10, p=0.049, Pearson's correlation coefficient = 0.634) (Figure 7D). These data suggest that while both the K^+ and the H^- tag the verrucae, the K^+ is a more faithful marker of verrucae, which was also visually evident in Figure 1, where the K^+ in panel 1C may more accurately mark verrucae than the H^- than in panel 1D. In summary, we found that AreaNorm($K^{+/-}$) correlated with verrucae height *and* volume while the AreaNorm($H^{+/-}$) correlated with only verrucae height.

DISCUSSION

In this report, we demonstrated that both Gaussian K and mean H curvature measures correlate with quantitative measures of entorhinal verrucae derived from manual and individual labeling. Specifically, the AreaNorm($H^{+/-}$) correlated best with verrucae height while AreaNorm($K^{+/-}$) correlated well with both verrucae height *and* volume. We also verified that entorhinal curvatures were significantly different from non-entorhinal curvatures and this finding paralleled our quantitative data measures.

The innovation of this study includes several facets. Most importantly, we have shown that semi-automatically derived measures can be used to quantify the geometry of entorhinal verrucae, that has significant implications for staging of diseases such as Alzheimer's. The H and K AreaNorm correlations with individual quantitative verrucae measures provide validation to curvature measures, especially given that H and K distinguish entorhinal from non-entorhinal cortices.

Our data show that K and H curvature correlates with quantitative verrucae metrics derived from manual labeling, suggesting these curvature measures can be used to predict verrucae size. All AreaNorm functions (both H and K) showed strong correlations with verrucae height; thus, making verrucae height the most distinguishing feature among our quantitative measures. Verrucae volume was significantly correlated as well, but less strongly, and only with the intrinsic curvature, K. It is remarkable that the AreaNorm functions of both the positive and negative H and K showed positive correlations with verrucae

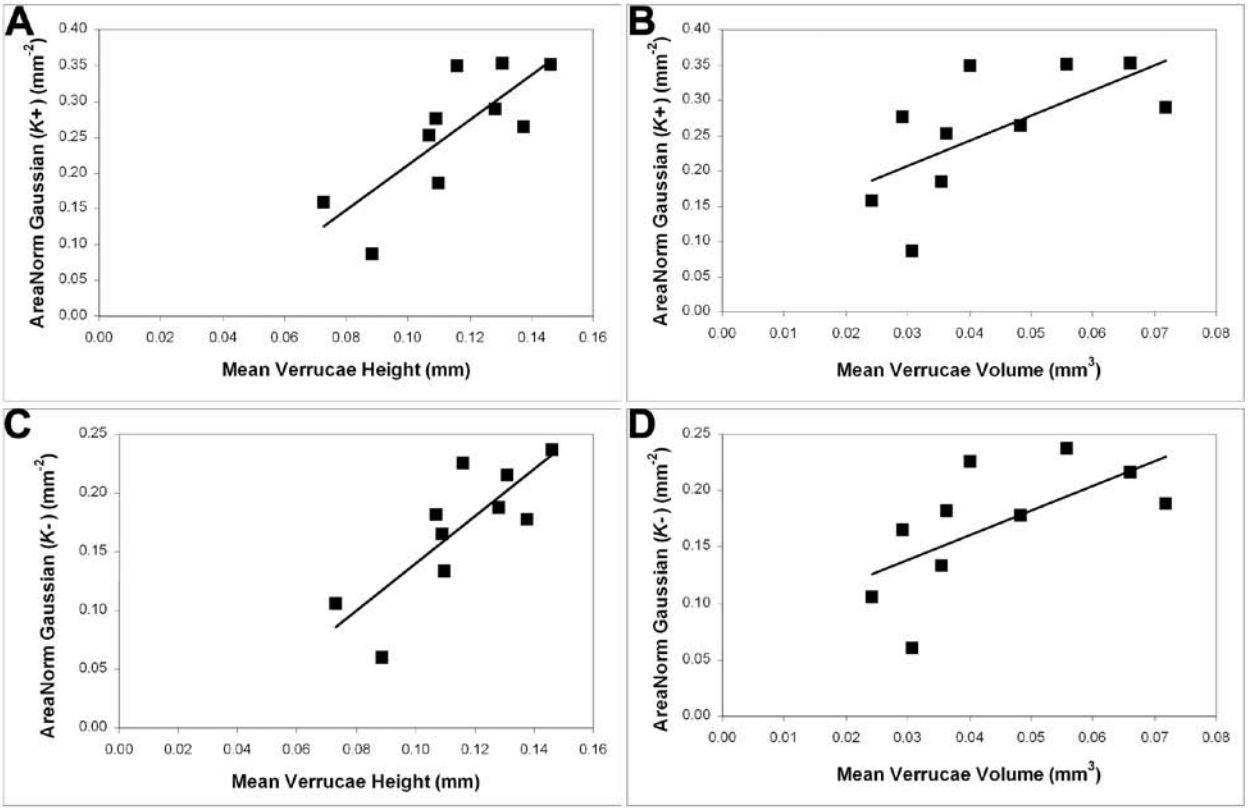

Figure 7. AreaNorm($K^{+/-}$) curvatures correlate to verrucae volume and height. AreaNorm(K^+) positively correlated with verrucae height (p=0.007) (A) and with verrucae volume (p=0.045) (B). AreaNorm(K^-) positively correlated with verrucae height (p=0.005) (C) and with verrucae volume (p=0.049) (D). Note that the K^+ characterizes spherical shapes irrespective of convexity, while K^- denotes a saddle (i.e. not a peak and not a trough).

geometry, suggesting that these curvature measures may be a more robust metric than manually labeling the verrucae because the entire geometry of the entorhinal cortex contributes to the measure, as opposed to the manual labeling which relies solely on the bumps. It is important to examine the positive and negative AreaNorm functions separately to avoid cancellation of the curvatures of the peaks and valleys on the surface[1]. It makes sense that the mean negative surface integral (H^-) has a stronger correlation with height than the positive surface integral (H^+) because for a surface with an outward-pointing normal vector field, outward bumps such as verrucae will have negative curvature (since a quadratic fit of the height of the surface in the normal direction over the tangent plane will have a negative coefficient of the quadratic term, such as a downward facing parabola). Given the spherical shape of the verrucae and the strong correlations with not only height but also volume, this may suggest that Gaussian curvature –either positive or negative- may be more predictive of actual verrucae prominence.

The biological significance of curvatures, *H* and *K,* with regard to the entorhinal verrucae size remains an intriguing question. By examining both intrinsic and extrinsic curvature, we collect more information about each surface. For H^-, we can examine the peaks only while the K^+ incorporates information from both peaks and troughs. Utilizing all the curvature maps (*H, K,* $^{+,-}$*),* we can build better models to address questions regarding the troughs (H^+, K^+), saddles (K^-) as well as the bumps (K^+, H^-) in non-demented aging samples. It may also suggest there is a small puckering or pit at the base of each verruca. Nonetheless, the intrinsic and extrinsic curvature measures can be extrapolated to the underlying cellular architecture. Verrucae (H^-) and (K^+) have large neurons beneath them while the troughs (H^+, *some* K^+) have cell sparse areas beneath them. Since these curvature values correlate with our previously published manual measurements, it could be speculated that these curvature measures may provide meaning to underlying neurons and may even reflect the cortico-cortical connectivity or loss of cortico-cortical connectivity if the neurons die as a result of disease.

It is well documented that verrucae disappear in Alzheimer's disease [3,6,33,34] and our previous study established that verrucae size is indicative of the degree of neurofibrillary tangle pathology that underlies the verrucae. The data presented here show that measures of surface curvature such as *K* and *H* may serve as morphometric biomarkers of the underlying neuropathology. It has been described that entorhinal verrucae increase in total number with increasing age [4]. It is enticing to further characterize a structure that may represent a morphological marker that increases with age but decreases with Alzheimer's disease.

There are limitations to this study. Although we have established a link between neuropathology of neurofibrillary tangles, a morphological structure and a metric like curvature that is potentially observable *in vivo*, the association is indirect. Of course, it is not possible to do *in vivo* neuropathology so this is the closest mechanism that is feasible. The extra *ex vivo* step is a substantial but a necessary and fruitful one. With current technology, it is difficult to obtain the *in vivo* resolutions required to directly resolve the entorhinal verrucae. We speculate that the resolution needed in MRI to resolve entorhinal verrucae *in vivo* would be approximately 250 µm isotropic but may be slightly lower (300 µm) if subject has large verrucae. As technology advances and higher resolution scans become conventional, the results presented here may lead to an additional *in vivo* measure that can be used for staging diseases such as Alzheimer's. Another limitation, albeit minor, is extraneous tissue, bubbles, and damaged tissue divots on the *ex vivo* surface and we must label around these artifacts to obtain an accurate measurement in some cases. If tissue debris was included, major outliers became evident. Thus, it is easy to observe the extraneous debris but an extra step in the methods to exclude it. Excessive debris did not occur in all cases, but it was notable in 4 out of the 10 cases (see Figure 5A,D,H and J) while tiny bubbles were noted in all cases. Since this model is *ex vivo* based and tissue is excised from the rest of the brain and handled, it is difficult to create a completely clean surface in this circumstance.

Curvature maps for entorhinal cortex with coincident histology assessment will advance our understanding of the verrucae biological function. Shape analysis and anatomical classification/validation will be an important next step for understanding the underlying cortical architecture in normal as well as diseased brains. Although current *in vivo* resolution cannot resolve these small structures, advances in MRI technology such high field strengths, surface array coils, and motion correction continue to improve resolution and contrast [35-39]. Until higher resolution *in vivo* is feasible where larger populations can be tested, *ex vivo* validation studies will lay the groundwork for verrucae function in the human brain.

Acknowledgements

We would like to thank those who donated brain tissue; their generous donation has made this work possible. We also thank Sita Kakunoori for MRI scanning, Ruopeng Wang for adding tools to Freeview, André van der Kouwe for sequence development and Lawrence L. Wald for solenoid coil construction and 7.0T support. Support for this research was provided in part by the National Center for Research Resources (P41-RR14075, and the NCRR BIRN Morphometric Project BIRN002, U24 RR021382), the National Institute for Biomedical Imaging and Bioengineering (R01EB006758), the National Institute on Aging (AG022381) and (AG028521), the National Center for Alternative Medicine (RC1AT005728-01), the National Institute for Neurological Disorders and Stroke (R01 NS052585-01, 1R21NS072652-01, 1R01NS070963), and was made possible by the resources provided by Shared Instrumentation Grants 1S10RR023401, 1S10RR019307, and 1S10RR023043. Additional support was provided by The Autism & Dyslexia Project funded by the Ellison Medical Foundation and by the NIH Blueprint for Neuro-science Research (U01-MH093765, part of the multi-institutional Human Connectome Project).

1 *As shown by the Gauss-Bonnet theorem, the integrated Gaussian curvature is a topological invariant of the surface and contains no information about surface geometry,*

References

[1] Retzius G., Das Menschenhirn, Stockholm: Norstedt and Sonhe, 1896

[2] Klinger J., Die makroskopische Anatomie der Ammonsformation, Denkschr. Schweiz. Naturforsch., 1948, 78, 82

[3] Augustinack J. C., Huber K. E., Postelnicu G. M., Kakunoori S., Wang R., van der Kouwe A. J., et al. Entorhinal verrucae geometry is coincident and correlates with Alzheimer's lesions: a combined neuropathology and high-resolution ex vivo MRI analysis, Acta Neuropathol., 2012, 123, 85-96

[4] Simic G., Bexheti S., Kelovic Z., Kos M., Grbic K., Hof P. R., et al., Hemispheric asymmetry, modular variability and age-related changes in the human entorhinal cortex, Neuroscience, 2005, 130, 911-925

[5] Van Hoesen G. W., Anatomy of the medial temporal lobe, Magn. Reson. Imaging., 1995, 13, 1047-1055

[6] Van Hoesen G. W., Solodkin A., Some modular features of temporal cortex in humans as revealed by pathological changes in Alzheimer's disease, Cereb. Cortex, 1993, 3, 465-475

[7] Todd P. H., A geometric model for the cortical folding pattern of simple folded brains, J. Theor. Biol., 1982, 97, 529-538

[8] Ball M. J., Lo P., Granulovacuolar degeneration in the ageing brain and in dementia, J. Neuropathol. Exp. Neurol., 1977, 36, 474-487

[9] Griffin L. D., The intrinsic geometry of the cerebral cortex, J. Theor. Biol., 1994, 166, 261-273

[10] Ronan L., Pienaar R., Williams G., Bullmore E., Crow T. J., Roberts N., et al., Intrinsic curvature: a marker of millimeter-scale tangential cortico-cortical connectivity?, Int. J. Neural Syst., 2011, 21, 351-366

[11] Pienaar R., Fischl B., Caviness V., Makris N., Grant P. E., A Methodology for analyzing curvature in the developing brain from preterm to adult, Int. J. Imaging Syst. Technol., 2008, 18, 42-68

[12] Armstrong E., Schleicher A., Omran H., Curtis M., Zilles K., The ontogeny of human gyrification, Cereb. Cortex, 1995, 5, 56-63

[13] Caviness V. S. Jr., Mechanical model of brain convolutional development, Science, 1975, 189, 18-21

[14] Van Essen D. C., Drury H. A., Structural and functional analyses of human cerebral cortex using a surface-based atlas, J. Neurosci., 1997, 17, 7079-7102

[15] Harris J. M., Whalley H., Yates S., Miller P., Johnstone E. C., Lawrie S. M., Abnormal cortical folding in high-risk individuals: a predictor of the development of schizophrenia?, Biol. Psychiatry, 2004, 56, 182-189

[16] Nordahl C. W., Dierker D., Mostafavi I., Schumann C. M., Rivera S. M., Amaral D. G., et al., Cortical folding abnormalities in autism revealed by surface-based morphometry, J. Neurosci., 2007, 27, 11725-11735

[17] Ochiai T., Grimault S., Scavarda D., Roch G., Hori T., Riviere D., et al., Sulcal pattern and morphology of the superior temporal sulcus, Neuroimage, 2004, 22, 706-719

[18] Rodriguez-Carranza C., Mukherjee P., Vigneron D., Barkovich J., Studholme C., A system for measuring regional surface folding of the neonatal brain from MRI, Med. Image Comput. Comput. Assist. Interv., 2006, 9, 201-208

[19] Yeo B. T., Yu P., Grant P. E., Fischl B., Golland P., Shape analysis with overcomplete spherical wavelets, Med. Image Comput. Comput. Assist. Interv., 2008, 11, 468-476

[20] Yu P., Grant P. E., Qi Y., Han X., Segonne F., Pienaar R., et al., Cortical surface shape analysis based on spherical wavelets, IEEE Trans. Med. Imaging., 2007, 26, 582-597

[21] Penttila J., Paillere-Martinot M. L., Martinot J. L., Ringuenet D., Wessa M., Houenou J., et al., Cortical folding in patients with bipolar disorder or unipolar depression, J. Psychiatry Neurosci., 2009, 34, 127-135

[22] Sallet P. C., Elkis H., Alves T. M., Oliveira J. R., Sassi E., Campi de Castro C., et al., Reduced cortical folding in schizophrenia: an MRI morphometric study, Am. J. Psychiatry, 2003, 160, 1606-1613

[23] Shim G., Jung W. H., Choi J. S., Jung M. H., Jang J. H., Park J. Y., et al., Reduced cortical folding of the anterior cingulate cortex in obsessive-compulsive disorder, J. Psychiatry Neurosci., 2009, 34, 443-449

[24] Thompson P. M., Lee A. D., Dutton R. A., Geaga J. A., Hayashi K. M., Eckert M. A., et al., Abnormal cortical complexity and thickness profiles mapped in Williams syndrome, J. Neurosci., 2005, 25, 4146-4158

[25] Van Essen D. C., Dierker D., Snyder A. Z., Raichle M. E., Reiss A. L., Korenberg J., Symmetry of cortical folding abnormalities in Williams syndrome revealed by surface-based analyses, J. Neurosci., 2006, 26, 5470-5483

[26] Whittle S., Allen N. B., Fornito A., Lubman D. I., Simmons J. G., Pantelis C., et al., Variations in cortical folding patterns are related to individual differences in temperament, Psychiatry Res., 2009, 172, 68-74

[27] Wisco J. J., Kuperberg G., Manoach D., Quinn B. T., Busa E., Fischl B., et al., Abnormal cortical folding patterns within Broca's area in schizophrenia: evidence from structural MRI, Schizophr. Res., 2007, 94, 317-327

[28] Yoon U., Lee J. M., Im K., Shin Y. W., Cho B. H., Kim I. Y., et al., Pattern classification using principal components of cortical thickness and its discriminative pattern in schizophrenia, Neuroimage, 2007, 34, 1405-1415

[29] Dale A. M., Fischl B., Sereno M. I., Cortical surface-based analysis. I. Segmentation and surface reconstruction, Neuroimage, 1999, 9, 179-194

[30] Fischl B., Sereno M. I., Dale A. M., Cortical surface-based analysis. II: Inflation, flattening, and a surface-based coordinate system, Neuroimage, 1999, 9, 195-207

[31] Fischl B., Sereno M. I., Tootell R. B., Dale A. M., High-resolution intersubject averaging and a coordinate system for the cortical surface, Hum. Brain Mapp., 1999, 8, 272-284

[32] Lorensen W. E., Cline H. E., Marching cubes: a high resolution 3D surface construction algorithm, Computer Graphics, 1987, 21

[33] Solodkin A., Van Hoesen G. W., Entorhinal cortex modules of the human brain, J. Comp. Neurol., 1996, 365, 610-617

[34] Van Hoesen G. W., Augustinack J. C., Dierking J., Redman S. J., Thangavel R., The parahippocampal gyrus in Alzheimer's disease. Clinical and preclinical neuroanatomical correlates, Ann. NY Acad. Sci., 2000, 911254-911274

[35] Augustinack J. C., van der Kouwe A. J., Blackwell M. L., Salat D. H., Wiggins C. J., Frosch M. P., et al., Detection of entorhinal layer II using 7Tesla magnetic resonance imaging, Ann. Neurol., 2005, 57, 489-494

[36] van der Kouwe A. J., Benner T., Dale A. M., Real-time rigid body motion correction and shimming using cloverleaf navigators, Magn. Reson. Med., 2006, 56, 1019-1032

[37] van der Kouwe A. J., Benner T., Salat D. H., Fischl B., Brain morphometry with multiecho MPRAGE, Neuroimage, 2008, 40, 559-569

[38] Wiggins G. C., Potthast A., Triantafyllou C., Wiggins C. J., Wald L. L., Eight-channel phased array coil and detunable TEM volume coil for 7 T brain imaging, Magn. Reson. Med., 2005, 54, 235-240

[39] Wiggins G. C., Triantafyllou C., Potthast A., Reykowski A., Nittka M., Wald L. L., 32-channel 3 Tesla receive-only phased-array head coil with soccer-ball element geometry, Magn. Reson. Med., 2006, 56, 216-223